

Towards the assimilation of satellite reflectance into semi-distributed ensemble snowpack simulations

Bertrand Cluzet^a, Jesus Revuelto^a, Matthieu Lafaysse^a, François Tuzet^{a,b}, Emmanuel Cosme^b, Ghislain Picard^b, Laurent Arnaud^b, Marie Dumont^a


^a*Univ. Grenoble Alpes, Université de Toulouse, Météo-France, CNRS, Centre d'Études de la Neige, Grenoble, France*

^b*Institut des Géosciences de l'Environnement, IGE, UGA-CNRS, Grenoble, France*

Abstract

Uncertainties of snowpack models and of their meteorological forcings limit their use by avalanche hazard forecasters, or for glaciological and hydrological studies. The spatialized simulations currently available for avalanche hazard forecasting are only assimilating sparse meteorological observations. As suggested by recent studies, their forecasting skills could be significantly improved by assimilating satellite data such as snow reflectances from satellites in the visible and the near-infrared spectra. Indeed, these data can help constrain the microstructural properties of surface snow and light absorbing impurities content, which in turn affect the surface energy and mass budgets. This paper investigates the prerequisites of satellite data assimilation into a detailed snowpack model. An ensemble version of Météo-France operational snowpack forecasting system (named S2M) was built for this study. This operational system runs on topographic classes instead of grid points, so-called 'semi-distributed' approach. Each class corresponds to one of the 23 mountain massifs of the French Alps (about 1000km² each), an altitudinal range (by step of 300m) and aspect (by step of 45°). We assess the feasibility

Email address: bertrand.cluzet@meteo.fr (Bertrand Cluzet)

 ©2019 by the author(s). Distributed under a Creative Commons CC-BY-NC-ND licence.

of satellite data assimilation in such a semi-distributed geometry. Ensemble simulations are compared with satellite observations from MODIS and Sentinel-2, and with in-situ reflectance observations. The study focuses on the 2013-2014 and 2016-2017 winters in the Grandes-Rousses massif. Substantial Pearson R^2 correlations (0.75-0.90) of MODIS observations with simulations are found over the domain. This suggests that assimilating it could have an impact on the spatialized snowpack forecasting system. However, observations contain significant biases (0.1-0.2 in reflectance) which prevent their direct assimilation. MODIS spectral band ratios seem to be much less biased. This may open the way to an operational assimilation of MODIS reflectances into the Météo-France snowpack modelling system.

Keywords: Snowpack Modelling, Ensemble, Spatialization, MODIS, Sentinel-2, Assimilation

Highlights

- Ensemble simulations of the snowpack are compared with satellite reflectances
- Spatial aggregation into the semi-distributed geometry filters the observation noises
- Satellite reflectances carry useful information worth to assimilate
- MODIS reflectances can not be directly assimilated because they are biased
- Ratios of MODIS reflectances show no evidence of bias and could be assimilated

1. Introduction

The avalanche forecasting services of some countries use a chain composed of meteorological forcings, coming from either a Numerical Weather Prediction model (NWP) or observations, and a detailed multilayer snowpack model such as Crocus (Vionnet et al.,

2012) or SNOWPACK (Lehning et al., 2002). Both meteorological forcings and snowpack modelling induce errors and uncertainties in the simulations (Essery et al., 2013; Vernay et al., 2015; Raleigh et al., 2015; Günther et al., 2019). These errors are considerably limiting the use of snowpack models by avalanche hazard forecasters (Morin et al., 2018). The representativeness of simulations is also limited in complex mountain terrain (Fiddes and Gruber, 2012). In addition, most of these snowpack modelling chains do not operationally assimilate any available information on the snowpack properties (either in-situ or remotely-sensed) (Helmert et al., 2018). There are several reasons for that : (1) snowpack in-situ observations are sparse and lack representativeness (2) satellite observations retrieval is challenging (Nolin, 2011; Helmert et al., 2018), (3) preserving state variable consistency within detailed snowpack models, which is a key point for avalanche forecasting, requires sophisticated assimilation algorithms (Magnusson et al., 2017). As a consequence, the errors often accumulate along the snow season leading to increasingly poor model performance and utility for avalanche hazard forecasting and other operational applications.

Data assimilation systems using ensemble approaches is the best way to reduce snowpack modelling errors (Charrois et al., 2016; Larue et al., 2018; Piazzzi et al., 2018; Winstral et al., 2019). The Particle Filter (PF) ensemble assimilation algorithm seems to be especially well suited to reduce detailed snowpack modelling errors (Magnusson et al., 2017). Indeed, ensembles enable to quantify the uncertainties of (1) meteorological forcings, using physically based ensembles (Vernay et al., 2015) or statistical perturbations (Charrois et al., 2016; Winstral et al., 2019), and (2) snowpack modelling, using multi-physical systems (Essery, 2015; Lafaysse et al., 2017). Charrois et al. (2016) did the first application of a PF within a detailed snowpack model, but only at one specific location and their ensemble only described the meteorological uncertainty, not model uncertainty.

They were followed by Magnusson et al. (2017) and Larue et al. (2018). Recently, Piazzini et al. (2018) and Smyth et al. (2019) applied the PF to a combination of meteorological and model ensembles, but with a less complex model and at the local scale as well. In parallel, spatialized application of PF has been done in several studies (Thirel et al., 2013; Baba et al., 2018), but with deterministic and low complexity snow models, not suited for avalanche hazard forecasting. This paper fills a gap by implementing a combination of a meteorological ensemble and a multiphysical system of detailed snow models in a spatialized context.

Daily moderate-resolution observations (250 to 500 m) in the visible (VIS) and near infra-red (NIR) spectrum from the MODerate Resolution Imaging Spectroradiometer (MODIS) are suitable to monitor the snowpack properties (Hall et al., 2002). Sentinel-2 (S2) has a coarser revisit time (5 days) but captures much finer spatial scales (10-20 m). From MODIS and S2 spectral Top Of Atmosphere (TOA) radiance products, it is possible to retrieve the snowpack extent as a Snow Cover Fraction by pixel (SCF) and Bottom of Atmosphere (BOA) reflectances which requires to account for the complexity of the radiative transfer in mountainous area (Richter, 1998; Sirguey, 2009). Many studies focus on the assimilation of SCF, showing a strong impact of assimilation in hydrological models (De Lannoy et al., 2012; Thirel et al., 2013; Stigter et al., 2017; Aalstad et al., 2018; Baba et al., 2018). However, SCF is expected to be of less interest for detailed snowpack modelling in alpine terrain, because the information content is limited to the snow line (Andreadis and Lettenmaier, 2006; Toure et al., 2018). Meanwhile, it is expected for the BOA reflectances to carry useful information on the temporal and spatial variability of the snowpack surface properties such as Light Absorbing Particles concentration (LAP, $[\text{kg kg}_{\text{snow}}^{-1}]$) and snow microstructure (quantified by the Specific Surface Area, SSA, $[\text{m}^2 \text{kg}^{-1}]$) (Dozier et al., 2009; Kokhanovsky et al., 2018). Indeed, these

variables drive the shortwave (SW) radiation absorption of the snowpack, and thus carry crucial information on the snow surface energy budget (Skiles et al., 2018; Mauro et al., 2019). Moreover, monitoring the surface snow microstructure can help detect precipitation (solid and liquid) and melting events, while frequent observations of surface LAP contents can enable to constrain LAP vertical layering within the snowpack. In line with this, Charrois et al. (2016) showed that assimilating satellite reflectances could help reduce Snow Water Equivalent (SWE, $[\text{kg m}^{-2}]$) modelling uncertainties by up to 45%.

The most detailed snow models are also able to compute reflectances from the snowpack properties, through the use of a detailed radiative transfer (Libois et al., 2015; Skiles and Painter, 2019) and the explicit evolution of SSA (Carmagnola et al., 2013) and LAP (Tuzet et al., 2017). Such radiative transfer models play the role of observation operators, computing observation-like variables from the model state variables. However, modelling geometries often differ from the distributed geometry of satellite retrievals (Mary et al., 2013). For instance, Météo-France multilayer snowpack model Crocus is operationally applied on several topographical classes (by 300 m elevation bands, for 8 different aspects and 3 different slopes, so-called "semi-distributed" geometry) inside so-called "massif" regions of about 1000 km^2 (Durand et al., 1999; Lafaysse et al., 2013). This semi-distributed framework, with around 200 topographical classes, was proven to be sufficient to represent the main features of snowpack variability with topography compared to fully distributed simulations at 25 to 250 m resolution (Fiddes and Gruber, 2012; Revuelto et al., 2018). However, the feasibility of the assimilation of satellite reflectances in Crocus semi-distributed model using the PF ensemble data assimilation algorithm, still needs to be assessed.

The main objective of this paper is to assess the potential for semi-distributed assim-

ilation of satellite observations of snowpack reflectances into ensemble snowpack simulations. For that purpose, we present extended comparisons of openloop simulations (e.g. without assimilation) with satellite observations from MODIS and S2 aggregated in this geometry. Sec. 2 presents the data and the modelling framework, while Sec. 3 introduces the aggregation method and defines the points of comparison from the assimilation perspective. Then Sec. 4 presents the comparison results, which are discussed in Sec. 5.

2. Data and model

2.1. Case study

This study focuses on two snow seasons (2013-2014 and 2016-2017) in the Grandes-Rousses (see Fig. 1). The area of about 500 km² is located in the Central French Alps, and is characterized by a wide elevation range from the bottom of Romanche valley (about 700 m a.s.l.) to the top of Aiguilles d'Arve (3514 m a.s.l.). This specific massif was chosen because it encompasses the Col du Lautaret (2058 m a.s.l.), where field campaigns have been carried out since winter 2016-2017 close to an automatic weather station (Tuzet et al., 2019).

The two snow seasons have been selected because they show contrasted snow conditions. 2013-2014 is characterised by above average snow depths, with frequent snowfall events and two major dust deposition events (end of February, end of March) (Dumont et al., 2017; Di Mauro et al., 2015). 2016-2017 was a warm winter, without significant snowfall between late November and beginning of January, and early melting in spring. In addition, several minor dust deposition events occurred after the end of February according to MOCAGE outputs.

2.2. Digital Elevation Model (DEM) and landcover

2.2.1. DEM

Digital Elevation Models (DEM) of the study area are used here to retrieve satellite data and to perform a topographical aggregation of observations into the model semi-distributed geometry. For that purpose, DEM BD Alti®² (IGN25) from the French Geographical Institute (*Institut National de l'information Géographique et forestière*, IGN) with native 25 m resolution was used in this study at different scales : 125 m for the retrieval of MODIS images (IGN125) (see Sec. 2.3.1) and 250 m (IGN250) for the topographical aggregation. In addition, a different DEM from Shuttle Radar Topography Mission (SRTM, Farr et al. (2007)) with 90 m resolution (SRTM90) is employed in the retrieval of S2 data (see Sec. 2.3.2).

2.2.2. Land Cover

CORINE Land Cover database³ was used to filter the land cover types of the region. Only land cover types 321 (grassland), 322 (moorland), 332 (bare rocks), 333 (sparse vegetation) and 335 (glaciers and perennial snow) were considered valid, hence excluding forests, urbanized area, and water bodies from this study since both modelling and satellite retrieval are difficult in such areas (Gascoin et al., 2019).

2.3. Snow observations

2.3.1. MODIS observations

MODIS top of atmosphere radiance in the first seven spectral bands are available at 250 to 500 m spatial resolution depending on the channel (see. Tab. 1). As depicted in Fig. 2 and Tab. 1, reflectance in visible bands (1,3,4) is mostly affected by the impurities

²<http://professionnels.ign.fr/bdalti>

³<https://www.data.gouv.fr/fr/datasets/corine-land-cover-occupation-des-sols-en-france/>

content in snow (BC and dust) whereas it depends mostly on SSA in the near-infrared spectral bands (2,5,6,7) (Dozier et al., 2009).

We extracted and post-processed these data in a 36x41 km² region (23616 pixels of 250 m resolution, see Fig. 1) including the Grandes-Rousses and Col du Lautaret field site during 2013-2014 and 2016-2017 snow seasons with MODImLab retrieval algorithm. In such context of complex terrain, MODImLab retrieval algorithm (Sirguey, 2009) was shown to outperform other products in many studies (Dumont et al., 2012; Charrois et al., 2013)). Indeed, MODImLab accounts for atmospherical radiative transfer, direct and diffuse contribution, multiple topographical reflection, terrain shading and snow reflectance anisotropy (see. Fig. 3).

For mixed pixels, MODImLab's spectral unmixing algorithm computes the reflectance of the snow fraction of the pixel together with a Snow Cover Fraction (SCF). For all the pixels, resulting product is the bi-hemispherical reflectance (accounting in particular for snow Bidirectional Refletance Density Function (BRDF), (Dumont et al., 2011)), with 250 m resolution in all bands. MODImLab provides additional masks for shadows (self and cast, see Fig. 3) and clouds. For both snow seasons, dates with good geometrical acquisition properties (Sensor Zenithal Angle (SZA) $\leq 30^\circ$), and clear sky were selected (see Tab. A.1 in Appendix) in order to ensure a maximal accuracy, following Sirguey et al. (2016) and Charrois et al. (2016).

2.3.2. Sentinel-2 observations

S2 is an ESA-Copernicus satellite program operational since 2016, carrying a multi-spectral high resolution (10-20 m) VIS/NIR sensor with several bands coinciding with MODIS wavelengths (see Tab. 1 and Fig. 2). Sentinel-2 ground flat bi-hemispherical reflectance products (product FRE, assuming a Lambertian surface) are retrieved by the MAJA processor (Hagolle et al., 2017), which is similar to MODImLab. Snow masks are

retrieved by Let It Snow algorithm⁴ and distributed by Theia Land data center⁵ (Gascoin et al., 2019). Acquisition is done close to nadir, with $SZA \leq 10^\circ$. Seven clear sky dates were selected during the 2016-2017 snow season (see Tab. A.1 in Appendix).

2.3.3. *In-situ observations*

Autosolalb is a high accuracy instrument measuring snow bi-hemispherical reflectance in the VIS/NIR spectrum (200-1100 nm, 3 nm resolution) including MODIS bands 1-4 (Dumont et al., 2017). In-situ Autosolalb observations of snowpack bi-hemispherical reflectance were acquired at Col du Lautaret field site (see Fig. 1 for location) during 2016-2017 winter. The acquisition time step is 12 minutes and acquisition for 2016-2017 winter started on 2017, February 16th. For a given observation time (see Tab. A.1 in Appendix), observation was computed as the mean of all available measurements within +30/-30 minutes and corrected for local slope effects as in Dumont et al. (2017).

2.4. *Model*

In S2M (SAFRAN-SURFEX/ISBA/Crocus-MEPRA), the Meteo-France operational modelling system of the snowpack, meteorological forcings from SAFRAN analysis (Durand et al., 1993) are used as inputs to the coupled multilayer ground/snowpack model SURFEX/ISBA/Crocus (Vionnet et al., 2012). Ensemble versions for these two components were used here.

⁴http://tully.ups-tlse.fr/grizonnet/let-it-snow/blob/master/doc/tex/ATBD_CES-Neige.pdf

⁵CNES.; Gascoin, S.; Grizonnet, M.; Hagolle, O.; Salgues, G. Theia Snow collection, 2017

2.4.1. Ensemble of Meteorological Forcings

In SAFRAN, a meteorological guess from the NWP model ARPEGE is adjusted with weather observations within each massif on the semi-distributed geometry. Here, in order to represent the uncertainties of this analysis, an ensemble of 35 meteorological forcings was generated by stochastic perturbations on all the meteorological variables of the reference SAFRAN analysis for the Grandes-Rousses. Following Charrois et al. (2016), the magnitude of perturbations was adjusted by a local assessment of SAFRAN errors. SAFRAN does not provide impurities deposition fluxes. Therefore, LAP wet and dry deposition fluxes for BC and dust were extrapolated from MOCAGE chemistry-transport model (Josse et al., 2004) at Lautaret field site (see Fig. 1). For LAP fluxes, Tuzet et al. (2017) showed that the order of magnitude were badly captured by ALADIN-Climate chemistry-transport model (Nabat et al., 2015), while the timing of events was well captured. Similar behaviour was found with MOCAGE, with an over estimation of BC fluxes in particular. As a consequence, each of the 4 LAP fluxes variables, for each of the 35 members, was multiplied by a constant random factor along the forcing time period, following a lognormal law ($\mu = 0.01, \sigma = 10$) for BC, and ($\mu = 1, \sigma = 10$) for dust.

2.4.2. Ensemble of snow models

ESCROC (Lafaysse et al., 2017) is the multiphysical ensemble version of SURFEX/ISBA/Crocus handling 7774 different model configurations. For this study, the last developments of the radiative transfer model TARTES and LAP handling in Crocus were mandatory to properly model the snowpack reflectance (T17 option of radiative transfer, Tuzet et al. (2017)), which were not included in Lafaysse et al. (2017). An ensemble of 1944 members using T17 option, so-called "E1tartes" was built for this study, including all the physical options described by Lafaysse et al. (2017) except for options of solar radiation

absorption scheme.

2.4.3. Model chain

The ensemble modelling chain setup is summarized in Fig. 4. At the beginning of a simulation, 35 model configurations are randomly drawn from E1tartes. Each one is associated with a perturbed forcing file to perform the simulation for the whole year, totalling 35 different snowpack simulations.

3. Methods

3.1. Topographic aggregation

An aggregation process is used to adapt the observations to the model semi-distributed geometry with the aim of assimilation. Another added value of the aggregation is to reduce random observation errors and average out features that are not accounted for in the model (Hyer et al., 2011).

3.1.1. DEM and topographical classification

In our modelling framework, a topographical class C_i is described by a triplet (e_i, a_i, s_i) where the elevation $e_i \in [600, 900, \dots, 3600]$, the aspect $a_i \in [0, 45, 90, \dots, 315]$ (in degrees, clockwise from North), and the slope $s_i \in [20, 40]$ (in degrees). Flat classes are described by a triplet $(e_i, -, 0)$. In our case, there is a total of 187 different topographical classes. For each pixel p , a triplet (e, a, s) is computed from the IGN250 DEM (see Sec. 2.2.1) and thus is attributed to a topographical class. The classification rule is described as follows for tilted classes (Eq. 1) and for flat classes (Eq. 2):

$$p(e, a, s) \in C_i(e_i, a_i, s_i) \iff \begin{cases} e \in [e_i - 150, e_i + 150[\\ s \in [s_i - 10, s_i + 10[\\ a \in [a_i - 22.5, a_i + 22.5[\end{cases} \quad (1)$$

$$p(e, a, s) \in C_i(e_i, -, 0) \iff \begin{cases} e \in [e_i - 150, e_i + 150[\\ s < 10 \end{cases} \quad (2)$$

Note that this classification process excludes pixels steeper than 50 degrees where both modelling and remote sensing are unsound.

3.1.2. MODIS aggregation

An algorithm is used to aggregate MODIS distributed observations into semi-distributed observations in order to compare it with model outputs. In this process, a particular attention is paid to the validity and spatial representativeness of the observations, as described in Fig. 5. Regarding the validity, pixels with clouds, self/cast shadows, invalid CORINE land covers (see Sec. 2.2.2) as well as pixel lying outside the Grandes-Rousses are filtered out (A label in Fig. 5). Then for reflectance only, pixels with Snow Cover Fraction SCF_{pix} inferior to 0.85, are discarded (B), since MODISLab reflectance product is less accurate for mixed pixels (Mary et al., 2013). The product (B) is referred to as "distributed reflectance".

Finally, reflectance and SCF are aggregated into semi-distributed products by taking the median value within each class. In order to ensure the spatial representativeness of the aggregated observations, classes where the number of valid pixels is below ten and having less than 10% of pixels with reflectance observations are filtered out in this process (C and D). For the same reason, classes where the average Snow Cover Fraction SCF_{class} is inferior to 0.85 are masked for reflectance in a final step (E).

3.1.3. Sentinel-2 aggregation

S2 images were aggregated to the semi-distributed geometry in a similar process as for MODIS (see Sec. 3.1.2), as described in Fig. 6. In a first step, a validity masking is

performed on Theia L2B Snow Mask using Theia L2A Clouds and Geophysical masks (A). Then, we produce the distributed S2 product (B) by classifying using the IGN250 DEM and discarding non-snow pixels. The aggregated SCF value (D) was here computed as the ratio between snowy and valid populations, when the valid population was above 10 pixels and 10 % of the total population (as described in the previous paragraph). Finally, aggregated SCF was used to filter the semi-distributed reflectance (D) as in Sec. 3.1.2.

3.2. Assessing the feasibility of data assimilation

Data assimilation algorithms generally require that systematical bias between the ensemble and the observations is negligible for a proper functioning (Dee and Da Silva, 1998). In addition, for ensemble data assimilation such as the PF, the observation should usually lie within the ensemble envelope, otherwise the algorithm is likely to collapse (Charrois et al., 2016). Rank diagrams are commonly used in the ensemble forecasting community to check for both issues by computing the histogram of the position of the observation within the ensemble for all available dates and places (Hamill, 2001). Furthermore, apart from these considerations, correlations between ensemble and observations timeseries can help quantify the information content from observation and its potential for assimilation (Reichle et al., 2004). If timeseries are weakly correlated, this means that it is likely that observations carry substantial information valuable for the ensemble, but that data assimilation of such different datasets will be a difficult task.

In order to assess the potential of applying assimilation algorithms to our spatialized ensemble simulation, a thorough comparison of observed and openloop (i.e. without assimilation) simulated reflectances is carried out here : (1) We assess the consistency of the spatial and temporal variations of the ensemble and observations based on two examples (one date and one topographic class). (2) We evaluate the products against

in-situ observations, in order to detect systematic biases and errors. (3) We compute Pearson correlations (R) between the ensemble median and semi-distributed observations timeseries in a wide range of topographic classes, to have additional information on the potential of information. (4) We generalize the results by computing rank diagrams, looking for bias and observation position within the ensemble at the same time and over numerous topographic classes and dates.

4. Results

4.1. Comparison of observed and simulated variables

4.1.1. Spatial comparison on a specific date

Fig. 7 shows maps of NIR semi-distributed reflectance (MODIS band 2) for the two satellite products (MODIS and S2) and the ensemble mean on February 18-19th, 2017. All pixels within the same topographical class are attributed the same value, and in many classes, observations and model are masked out because of shadows.

MODIS and S2 remarkably agree on the snowpack extent, while the ensemble mean seems to overestimate it. Both satellite products show on average more contrasted and lower reflectance values than the model. However, MODIS and the model agree on the reflectance dependence on aspect (lower in South-Eastern slopes), contrary to S2.

4.1.2. Ensemble and satellite reflectance timeseries

Fig. 8 shows the timeseries of ensemble and observations in MODIS bands 4 (VIS) and 2 and 5 (NIR) for the two snow seasons, in 2400 m flat class. This specific class was chosen here because it is flat, above the tree line and with a long snow covered season, thus easing the comparison all along the snow season. Although there is a strong

departure among observations and simulations (0.1-0.2 in bands 4 and 2, 0.1 in band 5), consistent time variations can be seen between semi-distributed observations (green stars) and the ensemble median (blue stars), for example in December and January of both snow seasons for band 5. For 2013-2014 winter (Fig. 8 a,c,e), high values of reflectance in all bands during the mid-winter are consistent with the recent snowfall at observation dates during this period (fresh snow has a high SSA, thus a high reflectance as shown in Fig. 2. Decrease in reflectance in all bands from November 2013 to mid December and on January 12th is related with extended periods without snowfall as seen on the HS curve. At the end of the snow season, the snow melt causes a decrease in SSA (i.e. low reflectance in band 2 and 5) due to wet metamorphism (Carmagnola et al., 2014) . Meanwhile, two dust deposition events (end of February 2014, end of March 2014 in MOCAGE model) can explain drops in band 4 reflectance through an increase in the snowpack surface LAP content. All those events appear in both ensemble and observation timeseries as well as in simulated surface impurities concentrations (not shown). Season 2016-2017 (Fig. 8b,d,f) had few, intense snowfall and extended dry periods with clear sky, allowing observe more pronounced reflectance variations.

Regarding the ensemble behaviour, in the visible bands, the ensemble Inter-Quartile Range (IQR) (blue boxes) seems generally lower during 2013-2014 winter than in 2016-2017. For all bands, the IQR is reduced after a snowfall (0.01-0.02 in bands 4 and 2, 0.02-0.03 in band 5), and increases with the time elapsed since the last snowfall and all along the melting season (up to 0.1 in bands 4 and 2 and 0.05 in band 5).

However, the main feature here is the strong departure between the ensemble and MODIS observations. For almost all dates of both winters, the semi-distributed observation is under all the members of the ensemble in bands 4 and 2. This deviation is smaller in band 5. Note also that the distributed observations IQR (green boxes) is considerable, and notably lower in band 5 (0.02-0.05) than in bands 2 and 4 (0.05-0.1). Regarding S2

observations, (Fig. 8b,d), agreement of semi-distributed observations (red stars) with the ensemble is good for fresh snow (2016, December 1st) but a strong departure (0.1-0.2) appears after extended periods without snowfall (2016, December 31th for example). Furthermore, the IQR of S2 distributed observations (red boxes) is 2-3 times larger than for MODIS.

4.1.3. Comparison with in-situ measurements

Comparison with field measurements at Col du Lautaret (Height of Snow (HS) and reflectance in bands 4 and 2) is possible for the 2100 m a.s.l flat class during 2016-2017 winter (see Fig. 9). First and foremost, there is a strong bias of MODIS observations with respect to in-situ Autosolalb observations (about 0.2 in band 4 and 0.1-0.15 in band 2). However, their time variations reproduce the temporal pattern obtained from in-situ observations for example between March 20th and 27th when an increase of reflectance is occurring in both products.

Meanwhile, the ensemble reflectance generally has the same magnitude as the in-situ observations in both bands. In band 4, the in-situ observations lie within the ensemble for fresh snow, for example on February 18th, March 27th and April 3rd. In band 2, reflectance is underestimated by the ensemble for those dates, except on March 27th. In addition, most of the members are overestimating reflectance in both bands during early melt (11th and 13th of March), while the comparison of the ensemble median and in-situ observed HS (blue and orange lines in Fig. 9) show that melt might be underestimated in the model. On March 20th, ensemble band 4 reflectance generally decreases while band 2 increases, together with a light snowfall in the model. Meanwhile, in-situ observations of HS show that there was no snowfall for this date.

4.1.4. Comparison over all reliable topographical classes

To investigate the distribution of this bias over time and space, MODIS observed semi-distributed values were plotted against the ensemble median. We restricted this study to topographical classes where the observation process is the most reliable, i.e. with low probability of being mixed/rocky (20° maximal slope) and with large enough pixel populations over the whole snow seasons (1800-3000 m.a.s.l.). In bands 4 and 2, Figs. 10a and 10b show a strong deviation from the 1:1 line. Moreover, the value range in band 4 is much lower in the model (about 0.05) than in the observations (about 0.3). In band 5 (Fig. 10c), observations and model better align with the 1:1 line.

In order to refine this analysis over space, linear regressions were systematically carried out between the ensemble median and the semi-distributed observations for each band inside each reliable topographical class (e.g. computing regressions between timeseries of blue stars and green stars in Fig. 8). The associated Pearson R^2 , slope and intercept coefficients are shown in Figs. 11a and 11b for bands 2 and 5. In the absence of model or observational bias, Slope should be close to 1 and Intercept to 0.

In band 2, overall high and significant R^2 (0.75-0.85) are noted. Slope is generally > 1 , and Intercept < -0.4 . However, regression is close to identity in the sunny slopes (strong dependence on aspect) with higher correlations. Band 5 shows high and significant R^2 as well (about 0.8-0.9). Slope and Intercept moderately deviates from Identity (Slope < 1).

4.2. Spectral bands reflectance ratio

4.2.1. Timeseries comparison between the model and satellite products

The bias between observations and model described in Sec. 4.1 is likely to be problematic for data assimilation. Computing a ratio between the reflectances in two different

bands (so-called "band ratio") might reduce this issue.

To that aim, the ratios between bands 5 and 4 (r54) and bands 5 and 2 (r52) were computed for MODIS observations. To do so, each ratio was computed on every pixel of the distributed reflectance (label B in Fig. 5), and aggregated and masked with the same method as for raw reflectances.

Fig.12 shows the temporal evolution of these variables in the 2400 m flat class. Time variations of the ensemble median and semi-distributed observations have compatible values (for example in r54 0.6-0.7 for fresh snow, and 0.25-0.4 in the late season). In about 50% of the cases, the semi-distributed observation falls within the ensemble IQR (blue boxes) for r54. In addition, note that r52 and r54 signals are very similar, be it in the model or the observations.

4.2.2. Comparison over all the reliable classes

Fig. 13 shows the semi-distributed observations against the ensemble medians for the ratios for all the reliable classes and the two snow seasons as in Sec. 4.1.4. There is no notable systematic bias between the observed ratios and the modelled ones.

Statistics of linear regression in Figs. 14a, and 14b show high R^2 values generally above 0.85, similar to those for band 5 in Fig. 11b. More interestingly, regression parameters are now around identity (Slope=1, Intercept=0) which illustrates the better agreement (no systematic bias) of observations and model for these ratios. While correlation patterns are almost identical for r54 and r52, Slope parameter is generally more departing from identity for r52 than for r54, with a significant dependence on aspect (lower Slopes in sunny aspects).

4.3. Towards assimilation

Fig. 15a shows the rank diagram for the raw reflectance of band 4, over all considered dates and topographical classes of the two snow seasons. In this graph, the observations lie in rank 0 (under all members of the ensemble) about 60 % of the occurrences, consistently with the negative bias depicted in previous section. On the contrary, the rank diagram for band ratio r_{54} in Fig. 15b is highly improved with respect to band 4, the observation being in the ensemble 80 % of the occurrences. Result is similar for r_{52} (not shown). Though overestimation of frequency of ranks 0 (under the ensemble) and 36 (over the ensemble) denote that the ensemble dispersion is insufficient, the rank diagram is flat, all the ranks having similar frequencies.

5. Discussion

5.1. On the relevance of the comparison in the semi-distributed framework

The semi-distributed framework was chosen for the comparison between observed and simulated reflectances because it is the basis of the French operational snowpack modelling system, and considering that running this model on a 250m-grid requires about 100 times more computer resources. Since it is quite specific, the different types of errors in observations and simulations in this semi-distributed geometry must be discussed for a correct interpretation of our results. Within a topographical class, observations are affected by (1) natural variability, (2) retrieval errors and (3) classification errors. In particular, DEM errors and resolution have a strong impact in satellite retrievals via shadows and subgrid topography (Baba et al., 2019; Davaze et al., 2018), leading to about $\pm 10\%$ errors in broadband albedo for MODIS data (Dumont et al., 2012). Moreover, S2 data are particularly affected by the three sources, since the retrieval DEM (SRTM90) in the

MAJA processor is too coarse to capture the topographic variability at the scale of the pixels (10-20 m) and because the classification is done to an even much coarser scale (IGN250). The resulting intraclass variability of S2 and MODIS is particularly visible in Figs 7e, 8 and 9.

However, the resulting distributions of the observations within the classes are reasonably gaussian (see Fig. Appendix B.1), meaning that semi-distributed observations, aggregated by taking the median, should remove random unbiased noises and outliers.

From the model point of view, the ensemble approach in this study is expected to satisfactorily assess snowpack modelling errors by the combination of meteorological and multiphysical model ensembles. However the semi-distributed simulations can have a limited spatial representativeness due to the snowpack natural variability, for example when the snow line or rain-snow line lies within the topographic class. In the general case, though, we expect this issue to be of limited importance, in the line with other studies (Mary et al., 2013).

5.2. Assets and limits of the satellite products

Since we consider that the observation process is not reliable in shadowed area, we filter out many observations, thus reducing the amount of spatial information available for assimilation. This means that from November to February, North facing slopes will likely not be observed. Therefore, ensemble simulations would not be corrected there during this period, if the assimilation were to be carried out on each topographic class independently. This stresses the need for a spatially coherent data assimilation algorithm, e.g. assimilating all observed topographic classes at the same time, in order to spatially propagate the effect of assimilation and to avoid inconsistent spatial patterns. Furthermore, a spatially comprehensive assimilation of SCF would be needed beforehand

to detect topographic classes where the ensemble and observations disagree on the presence of snow and assess where reflectance can be compared, similarly as in Baba et al. (2018).

Observations are also affected by significant errors and biases that are problematic for assimilation. S2 reflectance observations suffer from two significant inconsistencies. (1) The dependence of reflectance on aspect is too strong and unexpected. Higher band 2 reflectance are obtained in South-Eastern slopes where SSA should preferentially decrease owing to sun exposure (causing a decrease in reflectance through enhanced metamorphism) and lower SZA (Fig. 7) (Warren, 1982). (2) Reflectance decrease with time in the absence of snowfall in the early 2016-2017 snow season is too pronounced (Fig. 8b and d). These two considerations can be explained by retrieval errors in the MAJA algorithm, probably owing to the representation of topography and atmosphere, which was not specifically designed for snow reflectance retrieval in complex terrain (Hagolle et al., 2017). In addition, the reflectance retrieval is also affected by the use in MAJA retrieval of a coarse DEM (SRTM90) compared to the native resolution of the data (10-20 m). For all those reasons, improvements in the retrieval of S2 absolute reflectance values is necessary before considering their future assimilation.

MODIS reflectance observations also have a strong bias with the model. This bias is unambiguously attributed to MODIS according to the comparison with in-situ observations (Fig. 9). It is much higher than the intraclass variability of the observations and the ensemble IQR. In addition, Figs. 10 and 11 show that this bias is well described by a linear function of reflectance which is rather invariant in space and well stable in time. However, MODIS semi-distributed product (median) seems consistent, because : (1) we demonstrate that the median of the observations within the topographical classes is a representative value of the distribution in the general case, (2) reflectance dependence

on aspect corresponds to the model one (Fig. 7) (3) date-to-date time variations notably match those of the ensemble, (4) these variations sometimes better matches in-situ observations than the ensemble, which proves that their information content is good (Fig. 9, in March). All these considerations give us good confidence in the intrinsic quality and information content of MODIS observations, but a solution to this bias is required for assimilation.

5.3. Assimilating band ratios

Biases are a common issue of snowpack remote sensing (Veyssière et al., 2019; Balsamo et al., 2018) and require a proper estimation or correction before assimilation. Many methods exist in the NWP community to correct for the bias or dynamically estimate it in a data assimilation system (Draper et al., 2015; Auligné et al., 2007). However, these methods would require either (1) to assume a non-biased model (2) a representative in-situ reflectance dataset to analyse and model the bias before correcting it on-line (3) extensive, representative, and continuous in-situ observations of snowpack variables to constrain satellite reflectance biases (4) additional data from other satellite sources (Balsamo et al., 2018). All of those suffer from limitations owing to the specificities of snowpack modelling and monitoring in a complex terrain, respectively : (1) snowpack reflectance modelling probably suffers from some biases (Tuzet et al., 2017) (2) absence of any operational network measuring in-situ snowpack reflectance (3) sparse in-situ snowpack measurements in general (4) lack of reliable reflectance retrieval from other satellite sources (as shown here for S2).

Therefore, computing reflectance ratios for assimilation could be an appropriate solution in the current state of the art, because it does not require any assumption on the

bias attribution (observations and/or model) and nature. Results show that this method outstandingly allows to unbiased the observations using r54 and r52 (Figs. 13 and 14). Furthermore, band ratios are at the core of snowpack surface properties retrieval from satellites (Lyapustin et al., 2009; Negi and Kokhanovsky, 2011; Dumont et al., 2014; Kokhanovsky et al., 2018). It is not clear, however, whether all the precious information content of reflectance variables is preserved when computing band ratios. Firstly, the correlation of the two unbiased ratios is very high (≥ 0.9), as already noted by (Lyapustin et al., 2009), and these variables have similar temporal variations than MODIS band 5 (only sensitive to SSA) (see Figs. 8e,f and 12), suggesting that some information on the LAP content might be lost. Since it has been stated that reflectance assimilation requires at least two degrees of freedom, given the dependence of reflectance on LAP and SSA (Charrois et al., 2016), further work is required to infer whether these band ratios are varying sufficiently between polluted and pristine snowpacks. Other band combinations, with a higher sensitivity to LAP could also be used (if unbiased), as implemented in Di Mauro et al. (2015).

Nevertheless, rank diagrams are greatly improved compared to reflectance variables (Fig. 15). The obtained almost flat rank diagram for r54 shows that this variable is very likely to fall within the ensemble without any preferential position, for any topographical class and date. This is really encouraging towards spatialized assimilation of such variables.

5.4. *Ensemble modelling*

The remaining underdispersion of the ensemble evidenced by the over representation of the extremal positions in the rank diagrams, could be improved in the near future by a better characterization of the modelling chain uncertainties. (1) Increasing the amplitude of meteorological/impurities fluxes perturbations (Charrois et al., 2016) or using physi-

cal NWP ensemble such as PEARP (Descamps et al., 2015; Vernay et al., 2015) could allow to better account for NWP modelling uncertainties and intra-massif variability of weather conditions. (2) Including recent developments in Crocus such as blowing snow within the semi-distributed geometry (SYTRON, (Vionnet et al., 2018)) (3) Including different impurities scavenging parameter and optical properties configurations within the multiphysical ensemble (Tuzet et al., 2017).

Furthermore, adaptations to the presented ensemble modelling chain could make it more suitable for assimilation. First, the ensemble population ($N = 35$) is small compared to recent local ensemble assimilation attempts in snowpack modelling (e.g. Piazzini et al. (2018), Larue et al. (2018), Charrois et al. (2016)). However ensemble size must be kept to reasonable values for larger scale operational applications, and scores are not expected to highly depend on ensemble size for openloop simulations (Leutbecher, 2018). In addition, though increasing the ensemble population would allow to run several combinations of the forcings with ESCROC members, note that combining each forcing member with only one physical configuration of the model, therefore limiting the combinations, is a current practice in NWP to sample uncertainties (Descamps et al., 2015). Secondly, the choice of randomly drawing "N" ESCROC configurations versus carefully building a given subset of "N" members can be discussed. Indeed, Lafaysse et al. (2017) showed that the ensemble error representativeness could be improved by an appropriate optimized sample of members. However, this sample could not be tested here because it did not include T17 radiative transfer option (Tuzet et al., 2017), mandatory for reflectance modelling. Moreover, site-specific calibrations are expected to be suboptimal when applied over a wide diversity of sites (Krinner et al., 2018).

6. Conclusions

This study investigated the potential for assimilation of MODIS reflectance observations in ensemble snowpack simulations within a semi-distributed framework.

First, it is shown that MODIS observations of reflectance aggregated by topographic classes can be compared with semi-distributed ensemble simulation outputs, and that they convey substantial information content. However, it also clearly appears that MODIS observations are noisy and biased, due to the difficulty of retrieving surface reflectances in a complex terrain. In addition, it seems that S2 reflectance retrieval was affected by even bigger errors.

Meanwhile, it seems that the semi-distributed framework is particularly adapted to reflectance assimilation. First, it enables to efficiently remove observational noise thanks to aggregation within topographical classes. It is clear though, that monitoring the substantial intraclass natural variability of reflectance is then out of reach. Furthermore, state-of-the-art distributed snowpack modelling is currently not able to represent this spatial variability either. Reaching this goal would require the use of high resolution meteorological forcings (Quéno et al., 2016), and modelling of snow redistribution by wind and gravitation (Vionnet et al., 2014; Mott and Lehning, 2010; Freudiger et al., 2017) in distributed simulations. However, such simulations would require intensive computational resources compared to the semi distributed framework, added to the increase in computational cost due to ensemble forecasting already present here.

This study was also the first attempt of spatialized ensemble detailed snowpack modelling using a combination of meteorological and model ensembles. Results showed that

the semi-distributed setup is able to represent the associated errors and uncertainties in the modelling of reflectance well, and identified paths to make it more suitable to data assimilation.

Therefore, we are confident on the potential for assimilation to take full advantage of reflectance observations and detailed snowpack modelling in such a geometry. However, the remaining strong bias in MODIS semi-distributed reflectance observations prevents from directly assimilating them. A workaround was proposed for MODIS bias by computing ratios of reflectances, a simple method that should preserve the observations information content. We are confident that assimilating such variables is possible and could be beneficial for snowpack modelling in the near future. Furthermore, efforts to improve the retrieval of reflectances in complex terrain must be conducted, in order to reduce retrieval errors and bias, and implement retrieval of other medium-resolution satellite sources such as VIIRS and Sentinel3.

Acknowledgements

CNRM/CEN is part of Labex OSUG@2020 (investissement d'avenir – ANR10 LABX56). This study was partly supported by the ANR program ANR-16-CE01-0006 EBONI, LEFE ASSURANCE and APR MIOSOTIS. The authors are grateful to Lautaret staff and Station Alpine Joseph Fourier (SAJF) for ensuring a proper working of the instruments and support for in-situ experiments, P. Sirguey for providing MODImLab code and helpful discussions on retrieval algorithm, and to S. Gascoin, for advice and comments on the handling of Sentinel-2 data. J. Revuelto is supported by a Post-doctoral Fellowship of the AXA research fund (le Post-Doctorant Jesús Revuelto est bénéficiaire d'une bourse postdoctorale du Fonds AXA pour la Recherche Ref: CNRM 3.2.01/17).

Data and code availability

The datasets analysed during this study and the code used to produce the figures are available from the corresponding author on request. ESCROC is developed inside the open source SURFEX project (<http://www.umr-cnrm.fr/surfex>). While it is not implemented in an official SURFEX release, the code can be downloaded from the specific branch of the git repository maintained by Centre d'Études de la Neige. The full procedure and documentation can be found at https://opensource.umr-cnrm.fr/projects/snowtools_git/wiki/Procedure_for_new_users and https://opensource.umr-cnrm.fr/projects/snowtools_git/wiki/Data_assimilation_of_snow_observations. For reproducibility of results, the version used in this work is tagged as cluzetCRST. Processing of the albedo images has been performed using the open-source MODImLab algorithm, (version 1.2.5.d). This algorithm can be accessed by contacting its administrator, P. Sirguey.

References

References

Aalstad, K., Westermann, S., Schuler, T. V., Boike, J., Bertino, L., jan 2018. Ensemble-based assimilation of fractional snow-covered area satellite retrievals to estimate the snow distribution at arctic sites. *The Cryosphere* 12 (1).

URL <https://doi.org/10.5194/2Ftc-12-247-2018>

Andreadis, K. M., Lettenmaier, D. P., 2006. Assimilating remotely sensed snow observations into a macroscale hydrology model. *Advances in water resources* 29 (6), 872–886.

Auligné, T., McNally, A., Dee, D., 2007. Adaptive bias correction for satellite data in a numerical weather prediction system. *Quarterly Journal of the Royal Meteorological Society* 133 (624), 631–642.

Baba, M., Gascoin, S., Hanich, L., dec 2018. Assimilation of sentinel-2 data into a snowpack model in the high atlas of morocco. *Remote Sensing* 10 (12), 1982.

URL <https://doi.org/10.3390/2Frs10121982>

Baba, M. W., Gascoin, S., Kinnard, C., Marchane, A., Hanich, L., jul 2019. Effect of digital elevation model resolution on the simulation of the snow cover evolution in the high atlas. *Water Resources Research* 55 (7), 5360–5378.

URL <https://doi.org/10.1029/2F2018wr023789>

Balsamo, G., et al., 2018. Satellite and in situ observations for advancing global earth surface modelling: A review. *Remote Sensing* 10 (12).

URL <http://www.mdpi.com/2072-4292/10/12/2038>

Carmagnola, C. M., Domine, F., Dumont, M., Wright, P., Strellis, B., Bergin, M., Dibb, J., Picard, G., Libois, Q., Arnaud, L., Morin, S., 2013. Snow spectral albedo at summit,

- greenland: measurements and numerical simulations based on physical and chemical properties of the snowpack. *The Cryosphere* 7 (6), 1139–1160.
- Carmagnola, C. M., Morin, S., Lafaysse, M., Domine, F., Lesaffre, B., Lejeune, Y., Picard, G., Arnaud, L., 2014. Implementation and evaluation of prognostic representations of the optical diameter of snow in the surfex/isba-crocus detailed snowpack model. *The Cryosphere* 8 (2), 417–437.
- Charrois, L., Cosme, E., Dumont, M., Lafaysse, M., Morin, S., Libois, Q., Picard, G., 2016. On the assimilation of optical reflectances and snow depth observations into a detailed snowpack model. *The Cryosphere* 10 (3), 1021–1038.
- Charrois, L., Dumont, M., Sirguey, P., Morin, S., Lafaysse, M., Karbou, F., 2013. Comparing different modis snow products with distributed simulation of the snowpack in the french alps. In: *Proceedings of the International Snow Science Workshop*. Innsbruck, Austria.
- Davaze, L., Rabatel, A., Arnaud, Y., Sirguey, P., Six, D., Letreguilly, A., Dumont, M., 2018. Monitoring glacier albedo as a proxy to derive summer and annual surface mass balances from optical remote-sensing data. *The Cryosphere* 12 (1), 271–286.
URL <https://www.the-cryosphere.net/12/271/2018/>
- De Lannoy, G. J., Reichle, R. H., Arsenault, K. R., Houser, P. R., Kumar, S., Verhoest, N. E., Pauwels, V. R., 2012. Multiscale assimilation of advanced microwave scanning radiometer–eos snow water equivalent and moderate resolution imaging spectroradiometer snow cover fraction observations in northern colorado. *Water Resources Research* 48 (1).

- Dee, D. P., Da Silva, A. M., 1998. Data assimilation in the presence of forecast bias. *Quarterly Journal of the Royal Meteorological Society* 124 (545), 269–295.
- Descamps, L., Labadie, C., Joly, A., Bazile, E., Arbogast, P., Cébron, P., 2015. Pearp, the météo-france short-range ensemble prediction system. *Quarterly Journal of the Royal Meteorological Society* 141 (690), 1671–1685.
- Di Mauro, B., Fava, F., Ferrero, L., Garzonio, R., Baccolo, G., Delmonte, B., Colombo, R., 2015. Mineral dust impact on snow radiative properties in the european alps combining ground, uav, and satellite observations. *Journal of Geophysical Research: Atmospheres* 120 (12), 6080–6097.
- Dozier, J., Green, R. O., Nolin, A. W., Painter, T. H., 2009. Interpretation of snow properties from imaging spectrometry. *Remote Sensing of Environment* 113, S25–S37.
- Draper, C., Reichle, R., De Lannoy, G., Scarino, B., 2015. A dynamic approach to addressing observation-minus-forecast bias in a land surface skin temperature data assimilation system. *Journal of Hydrometeorology* 16 (1), 449–464.
- Dumont, M., Arnaud, L., Picard, G., Libois, Q., Lejeune, Y., Nabat, P., Voisin, D., Morin, S., 2017. In situ continuous visible and near-infrared spectroscopy of an alpine snowpack. *The Cryosphere* 11 (3), 1091–1110.
- Dumont, M., Brun, E., Picard, G., Michou, M., Libois, Q., Petit, J., Geyer, M., Morin, S., Josse, B., 2014. Contribution of light-absorbing impurities in snow to greenland's darkening since 2009. *Nature Geoscience* 7 (7), 509.
- Dumont, M., Gardelle, J., Sirguey, P., Guillot, A., Six, D., Arnaud, A. R. Y., 2012. Linking glacier annual mass balance and glacier albedo retrieved from modis data. *The Cryosphere* 6, 1527–1539.

- Dumont, M., Sirguey, P., Arnaud, Y., Six, D., 2011. Monitoring spatial and temporal variations of surface albedo on Saint Sorlin Glacier (French Alps) using terrestrial photography. *The Cryosphere* 5 (3), 759–771.
URL <http://www.the-cryosphere.net/5/759/2011/>
- Durand, Y., Brun, E., Mérindol, L., Guyomarc'h, G., Lesaffre, B., Martin, E., 1993. A meteorological estimation of relevant parameters for snow models. *Ann. Glaciol.* 18, 65–71.
- Durand, Y., Giraud, G., Brun, E., Mérindol, L., Martin, E., 1999. A computer-based system simulating snowpack structures as a tool for regional avalanche forecasting. *J. Glaciol.* 45 (151), 469–484.
- Essery, R., 2015. A factorial snowpack model (fsm 1.0). *Geosci. Model Dev.* 8, 3867–3876.
- Essery, R., Morin, S., Lejeune, Y., Bauduin-Ménard, C., 2013. A comparison of 1701 snow models using observations from an alpine site. *Adv. Water Res.* 55, 131–148.
- Farr, T. G., Rosen, P. A., Caro, E., Crippen, R., Duren, R., Hensley, S., Kobrick, M., Paller, M., Rodriguez, E., Roth, L., et al., 2007. The shuttle radar topography mission. *Reviews of geophysics* 45 (2).
- Fiddes, J., Gruber, S., 2012. Toposub: a tool for efficient large area numerical modelling in complex topography at sub-grid scales. *Geoscientific Model Development* 5 (5), 1245–1257.
URL <http://www.geosci-model-dev.net/5/1245/2012/>
- Freudiger, D., Kohn, I., Seibert, J., Stahl, K., Weiler, M., 2017. Snow redistribution for

- the hydrological modeling of alpine catchments. *Wiley Interdisciplinary Reviews: Water* 4 (5), e1232.
- Gascoin, S., Grizonnet, M., Bouchet, M., Salgues, G., Hagolle, O., 2019. Theia snow collection: high-resolution operational snow cover maps from sentinel-2 and landsat-8 data. *Earth System Science Data* 11 (2), 493–514.
- Günther, D., Marke, T., Essery, R., Strasser, U., 2019. Uncertainties in snowpack simulations—assessing the impact of model structure, parameter choice, and forcing data error on point-scale energy balance snow model performance. *Water Resources Research* 55 (4), 2779–2800.
- Hagolle, O., Huc, M., Descardins, C., Auer, S., Richter, R., 2017. Maja algorithm theoretical baseline document. Tech. rep.
- Hall, D. K., Riggs, G. A., Salomonson, V. V., DiGirolamo, N. E., Bayr, K. J., 2002. Modis snow-cover products. *Remote sensing of Environment* 83 (1-2), 181–194.
- Hamill, T., 2001. Interpretation of rank histograms for verifying ensemble forecasts. *Mon. Weather Rev.* 129 (3), 550–560.
- Helmert, J., Şensoy Şorman, A., Alvarado Montero, R., De Michele, C., de Rosnay, P., Dumont, M., Finger, D., Lange, M., Picard, G., Potopová, V., et al., 2018. Review of snow data assimilation methods for hydrological, land surface, meteorological and climate models: Results from a cost harmonosnow survey. *Geosciences* 8 (12), 489.
- Hyer, E., Reid, J., Zhang, J., 2011. An over-land aerosol optical depth data set for data assimilation by filtering, correction, and aggregation of modis collection 5 optical depth retrievals. *Atmospheric Measurement Techniques* 4 (3), 379–408.

- Josse, B., Simon, P., Peuch, V.-H., 2004. Radon global simulations with the multiscale chemistry and transport model mocage. *Tellus B: Chemical and Physical Meteorology* 56 (4), 339–356.
- Kokhanovsky, A., Lamare, M., Mauro, B. D., Picard, G., Arnaud, L., Dumont, M., Tuzet, F., Brockmann, C., Box, J. E., 2018. On the reflectance spectroscopy of snow. *The Cryosphere* 12 (7), 2371–2382.
- Krinner, G., Derksen, C., Essery, R., Flanner, M., Hagemann, S., Clark, M., Hall, A., Rott, H., Brutel-Vuilmet, C., Kim, H., et al., 2018. Esm-snowmip: assessing snow models and quantifying snow-related climate feedbacks. *Geoscientific Model Development* 11, 5027–5049.
- Lafaysse, M., Cluzet, B., Dumont, M., Lejeune, Y., Vionnet, V., Morin, S., 2017. A multiphysical ensemble system of numerical snow modelling. *The Cryosphere* 11 (3), 1173–1198.
URL <https://www.the-cryosphere.net/11/1173/2017/>
- Lafaysse, M., Morin, S., Coléou, C., Vernay, M., Serça, D., Besson, F., Willemet, J.-M., Giraud, G., Durand, Y., 2013. Toward a new chain of models for avalanche hazard forecasting in french mountain ranges, including low altitude mountains. In: *Proceedings of the International Snow Science Workshop - Grenoble and Chamonix*. pp. 162–166.
- Larue, F., Royer, A., De Sève, D., Roy, A., Picard, G., Vionnet, V., Cosme, E., 2018. Simulation and assimilation of passive microwave data using a snowpack model coupled to a calibrated radiative transfer model over northeastern canada. *Water Resources Research* 54 (7), 4823–4848.
- Lehning, M., Bartelt, P., Brown, B., Fierz, C., Satyawali, P., 2002. A physical SNOW-

- PACK model for the Swiss avalanche warning. part II: snow microstructure. *Cold Reg. Sci. Technol.* 35 (3), 147 – 167.
- Leutbecher, M., oct 2018. Ensemble size: How suboptimal is less than infinity? *Quarterly Journal of the Royal Meteorological Society* 145 (S1), 107–128.
URL <https://doi.org/10.1002/qj.3387>
- Libois, Q., Picard, G., Arnaud, L., Dumont, M., Lafaysse, M., Morin, S., Lefebvre, E., 2015. Summertime evolution of snow specific surface area close to the surface on the Antarctic Plateau. *The Cryosphere* 9 (6), 2383–2398.
- Lyapustin, A., Tedesco, M., Wang, Y., Aoki, T., Hori, M., Kokhanovsky, A., 2009. Retrieval of snow grain size over greenland from modis. *Remote Sens. Environ.* 113 (9), 1976 – 1987.
- Magnusson, J., Winstral, A., Stordal, A. S., Essery, R., Jonas, T., 2017. Improving physically based snow simulations by assimilating snow depths using the particle filter. *Water Resources Research* 53 (2), 1125–1143.
- Mary, A., Dumont, M., Dedieu, J.-P., Durand, Y., Sirguey, P., Milhem, H., Mestre, O., Negi, H. S., Kokhanovsky, A. A., Lafaysse, M., Morin, S., 2013. Intercomparison of retrieval algorithms for the specific surface area of snow from near-infrared satellite data in mountainous terrain, and comparison with the output of a semi-distributed snowpack model. *The Cryosphere* 7, 741–761.
- Mauro, B. D., Garzonio, R., Rossini, M., Filippa, G., Pogliotti, P., Galvagno, M., Morra di Cella, U., Migliavacca, M., Baccolo, G., Clemenza, M., et al., 2019. Saharan dust events in the european alps: role in snowmelt and geochemical characterization. *The Cryosphere* 13 (4), 1147–1165.

- Morin, S., Fierz, C., Horton, S., Bavay, M., Coléou, C., Dumont, M., Gobiet, A., Hagenmuller, P., Lafaysse, M., Mitterer, C., Monti, F., Müller, K., Olefs, M., Snook, J. S., Techel, F., van Herwijnen, A., Vionnet, V., 2018. Application of physical snowpack models in support of operational avalanche hazard forecasting: a status report on current implementations and prospects for the future. In: Proceedings of the International Snow Science Workshop Innsbruck - 2018, 7-12 October, Innsbruck, Austria. pp. 1098–1107.
- Mott, R., Lehning, M., 2010. Meteorological modeling of very high-resolution wind fields and snow deposition for mountains. *Journal of Hydrometeorology* 11 (4), 934–949.
- Nabat, P., Somot, S., Mallet, M., Michou, M., Sevault, F., Driouech, F., Meloni, D., di Sarra, A., Di Biagio, C., Formenti, P., et al., 2015. Dust aerosol radiative effects during summer 2012 simulated with a coupled regional aerosol–atmosphere–ocean model over the mediterranean. *Atmospheric Chemistry and physics* 15 (6), 3303–3326.
- Negi, H., Kokhanovsky, A., 2011. Retrieval of snow albedo and grain size using reflectance measurements in himalayan basin. *The Cryosphere* 5 (1), 203–217.
- Nolin, A. W., 2011. Recent advances in remote sensing of seasonal snow. *J. Glaciol.* 56 (200), 1141–1150.
- Piazzì, G., Thirel, G., Campo, L., Gabellani, S., 2018. A particle filter scheme for multivariate data assimilation into a point-scale snowpack model in an alpine environment. *The Cryosphere* 12 (7), 2287–2306.
- Quéno, L., Vionnet, V., Dombrowski-Etchevers, I., Lafaysse, M., Dumont, M., Karbou, F., 2016. Snowpack modelling in the pyrenees driven by kilometric-resolution meteo-

- rological forecasts. *The Cryosphere* 10 (4), 1571–1589.
URL <https://www.the-cryosphere.net/10/1571/2016/>
- Raleigh, M. S., Lundquist, J. D., Clark, M. P., 2015. Exploring the impact of forcing error characteristics on physically based snow simulations within a global sensitivity analysis framework. *Hydrol. Earth Syst. Sci.* 19 (7), 3153–3179.
- Reichle, R. H., Koster, R. D., Dong, J., Berg, A. A., 2004. Global soil moisture from satellite observations, land surface models, and ground data: Implications for data assimilation. *Journal of Hydrometeorology* 5 (3), 430–442.
- Revuelto, J., Lecourt, G., Lafaysse, M., Zin, I., Charrois, L., Vionnet, V., Dumont, M., Rabatel, A., Six, D., Condom, T., et al., 2018. Multi-criteria evaluation of snowpack simulations in complex alpine terrain using satellite and in situ observations. *Remote Sensing* 10 (8), 1171.
- Richter, R., 1998. Correction of satellite imagery over mountainous terrain. *Applied optics* 37 (18), 4004–4015.
- Sirguey, P., 2009. Simple correction of multiple reflection effects in rugged terrain. *Int. J. Remote Sens.* 30, 1075–1081.
- Sirguey, P., Still, H., Cullen, N. J., Dumont, M., Arnaud, Y., Conway, J. P., 2016. Reconstructing the mass balance of brewster glacier, new zealand, using modis-derived glacier-wide albedo. *The Cryosphere* 10 (5), 2465–2484.
- Skiles, S. M., Flanner, M., Cook, J. M., Dumont, M., Painter, T. H., 2018. Radiative forcing by light-absorbing particles in snow. *Nature Climate Change*, 1.

- Skiles, S. M., Painter, T. H., 2019. Toward understanding direct absorption and grain size feedbacks by dust radiative forcing in snow with coupled snow physical and radiative transfer modeling. *Water Resources Research*.
- Smyth, E. J., Raleigh, M. S., Small, E. E., feb 2019. Particle filter data assimilation of monthly snow depth observations improves estimation of snow density and SWE. *Water Resources Research* 55 (2), 1296–1311.
URL <https://doi.org/10.1029%2F2018wr023400>
- Stigter, E. E., Wanders, N., Saloranta, T. M., Shea, J. M., Bierkens, M. F., Immerzeel, W. W., 2017. Assimilation of snow cover and snow depth into a snow model to estimate snow water equivalent and snowmelt runoff in a himalayan catchment. *The Cryosphere* 11 (4), 1647–1664.
- Thirel, G., Salamon, P., Burek, P., Kalas, M., 2013. Assimilation of modis snow cover area data in a distributed hydrological model using the particle filter. *Remote Sensing* 5 (11), 5825–5850.
- Toure, A. M., Reichle, R. H., Forman, B. A., Getirana, A., De Lannoy, G. J., 2018. Assimilation of modis snow cover fraction observations into the nasa catchment land surface model. *Remote Sensing* 10 (2), 316.
- Tuzet, F., Dumont, M., Arnaud, L., Voisin, D., Lamare, M., Larue, F., Revuelto, J., Picard, G., 2019. Influence of light-absorbing particles on snow spectral irradiance profiles. *The Cryosphere* 13 (8), 2169–2187.
- Tuzet, F., Dumont, M., Lafaysse, M., Picard, G., Laurent, A., Voisin, D., Lejeune, Y., Charrois, L., Nabat, P., Morin, S., 2017. A multilayer physically based snowpack model

- simulating direct and indirect radiative impacts of light-absorbing impurities in snow. *The Cryosphere* 11 (6), 2633.
- Vernay, M., Lafaysse, M., Merindol, L., Giraud, G., Morin, S., 2015. Ensemble forecasting of snowpack conditions and avalanche hazard. *Cold. Reg. Sci. Technol.* 120, 251–262.
- Veyssi re, G., Karbou, F., Morin, S., Lafaysse, M., Vionnet, V., 2019. Evaluation of sub-kilometric numerical simulations of c-band radar backscatter over the french alps against sentinel-1 observations. *Remote Sensing* 11 (1), 8.
- Vionnet, V., Brun, E., Morin, S., Boone, A., Martin, E., Faroux, S., Le-Moigne, P., Willemet, J.-M., 2012. The detailed snowpack scheme Crocus and its implementation in SURFEX v7.2. *Geosci. Model. Dev.* 5, 773–791.
- Vionnet, V., Guyomarc'h, G., Lafaysse, M., Naaime-Bouvet, F., Giraud, G., Deliot, Y., 2018. Operational implementation and evaluation of a blowing snow scheme for avalanche hazard forecasting. *Cold Regions Science and Technology* 147, 1–10.
- Vionnet, V., Martin, E., Masson, V., Guyomarc'h, G., Naaime-Bouvet, F., Prokop, A., Durand, Y., Lac, C., 2014. Simulation of wind-induced snow transport and sublimation in alpine terrain using a fully coupled snowpack/atmosphere model. *The Cryosphere* 8 (2), 395–415.
- Warren, S., 1982. Optical properties of snow. *Rev. Geophys.* 20 (1), 67–89.
- Winstral, A., Magnusson, J., Schirmer, M., Jonas, T., 2019. The bias-detecting ensemble: A new and efficient technique for dynamically incorporating observations into physics-based, multilayer snow models. *Water Resources Research* 55 (1), 613–631.

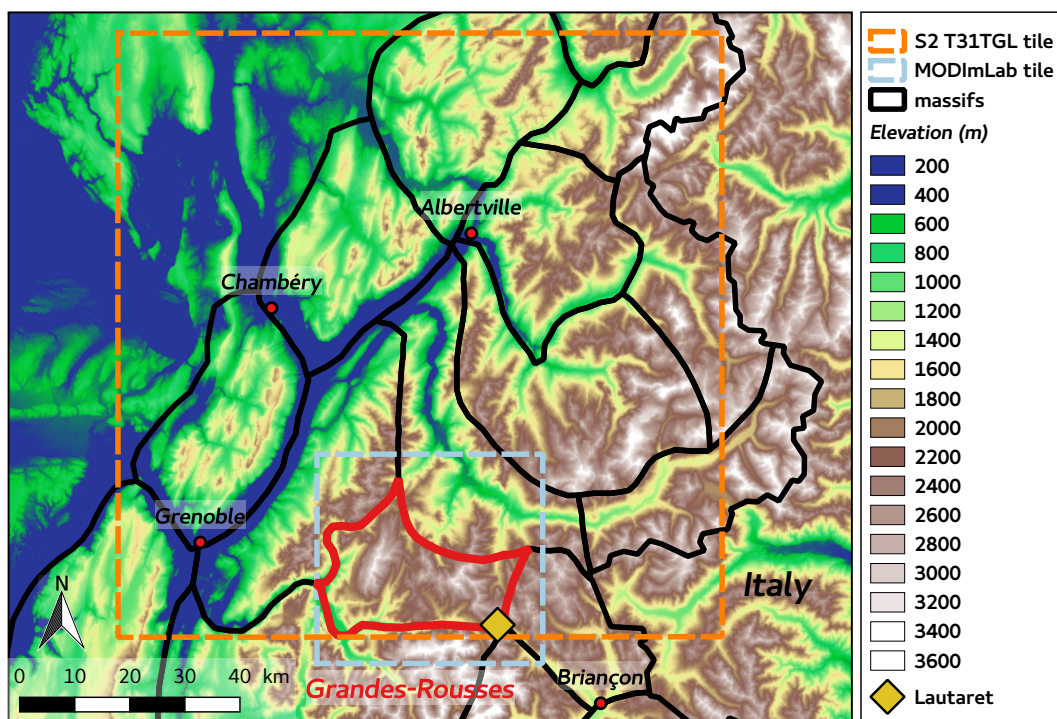


Figure 1: Map of the study area of the Grandes-Rousses (red), located in the central French Alps. Lautaret field site (diamond) and satellite retrieval tiles (boxes) are also indicated, together with the limits of other SAFRAN massifs (black). Source : Shuttle Radar Topography Mission (SRTM), resolution : 90m.

MODIS ID /S2 ID	B3/B2	B4/B3	B1/B4	B2/B8A	B5	B6/B11	B7/B12
Central Wavelength (<i>nm</i>)	469/497	555/560	645/665	858.5/865	1240	1640/1614	2130/2202
Bandwidth (<i>nm</i>)	20/100	20/45	50/40	35/33	20	24/143	50/242
Resol. at Nadir (<i>m</i>)	500/10	500/10	250/10	250/20	500	500/20	500
Spectral Domain	VIS	VIS	VIS	VIS/NIR	NIR	IR	IR
Sensitivity to LAP	++	++	++	+			
Sensitivity to SSA	+	+	+	++	+++	++	++
Penetration depth (<i>m</i>)	up to 10-20cm	a few cm	a few cm	a few cm	mm	mm	mm

Table 1: MODIS considered spectral band properties together with the closest matching Sentinel-2 band.

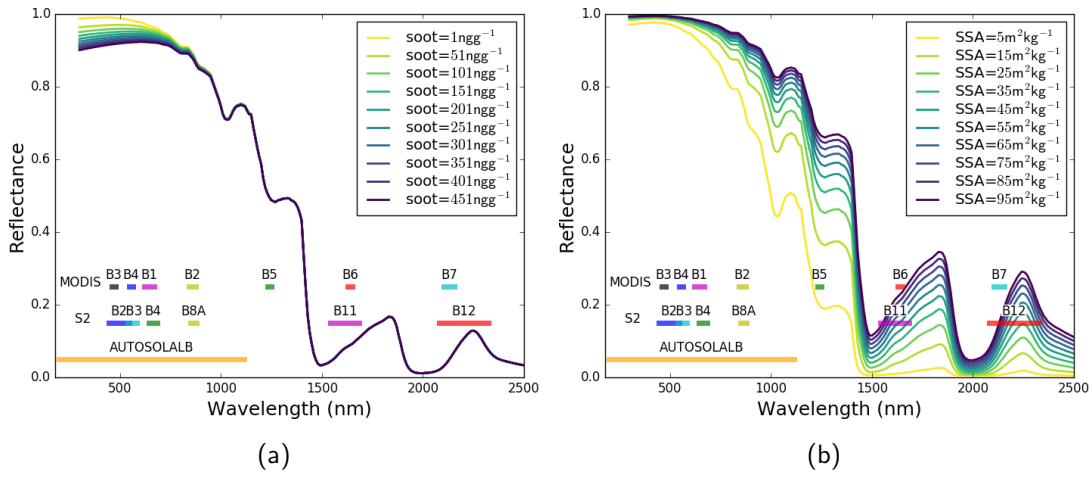


Figure 2: Computation of snow diffuse reflectances using TARTES for varying soot concentrations ($\text{SSA}=40\text{m}^2 \text{kg}^{-1}$) (2a) and varying SSA (2b), for 1 m of 300kg m^{-3} density uniform snowpack, together with MODIS and S2 spectral bands.

Source : <http://snowtartes.pythonanywhere.com>

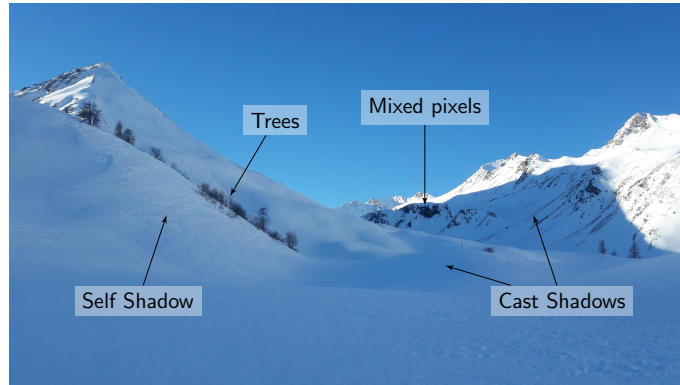


Figure 3: Example of the complexity of the retrieval of reflectance affected by shadows, trees, and mixed snow covers in a complex terrain. (Bertrand Cluzet, Col du Lautaret, December 20th 2017)

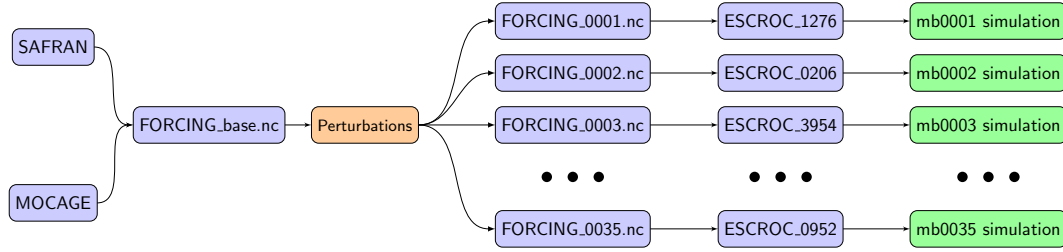


Figure 4: Setup of the ensemble modelling chain.

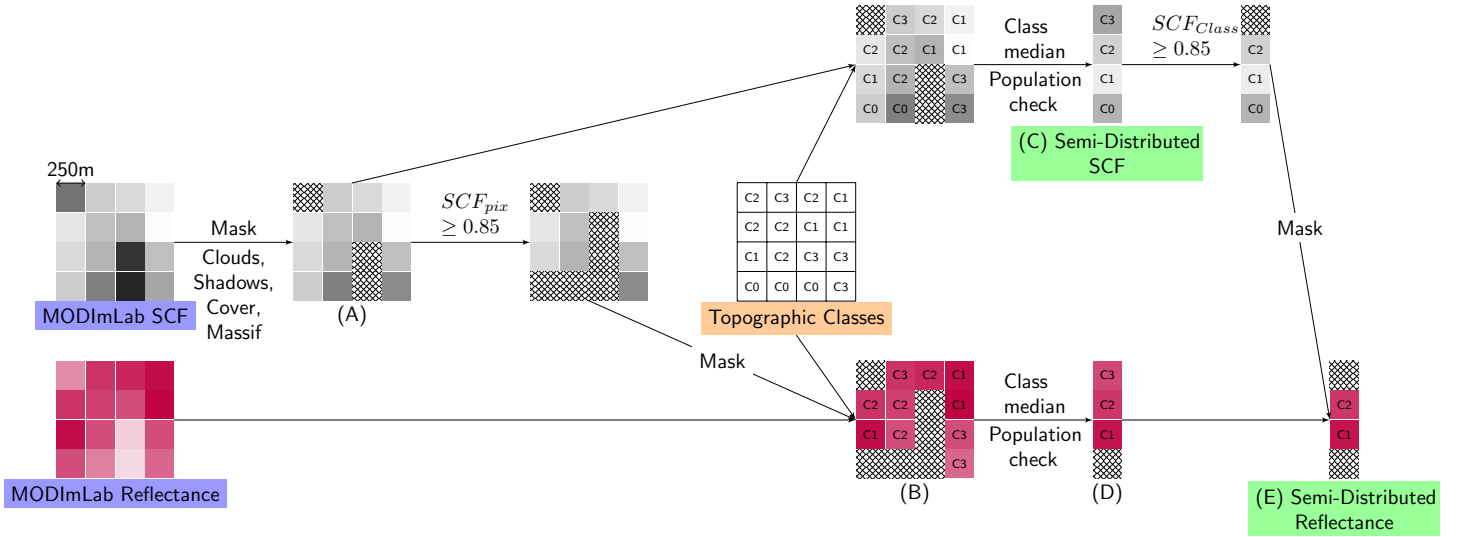


Figure 5: Flowchart of the conversion of MODImLab products (purple) to semi-distributed data (green), using the Topographical Classification (orange) from Sec. 3.1.1. Masked data are hatched.

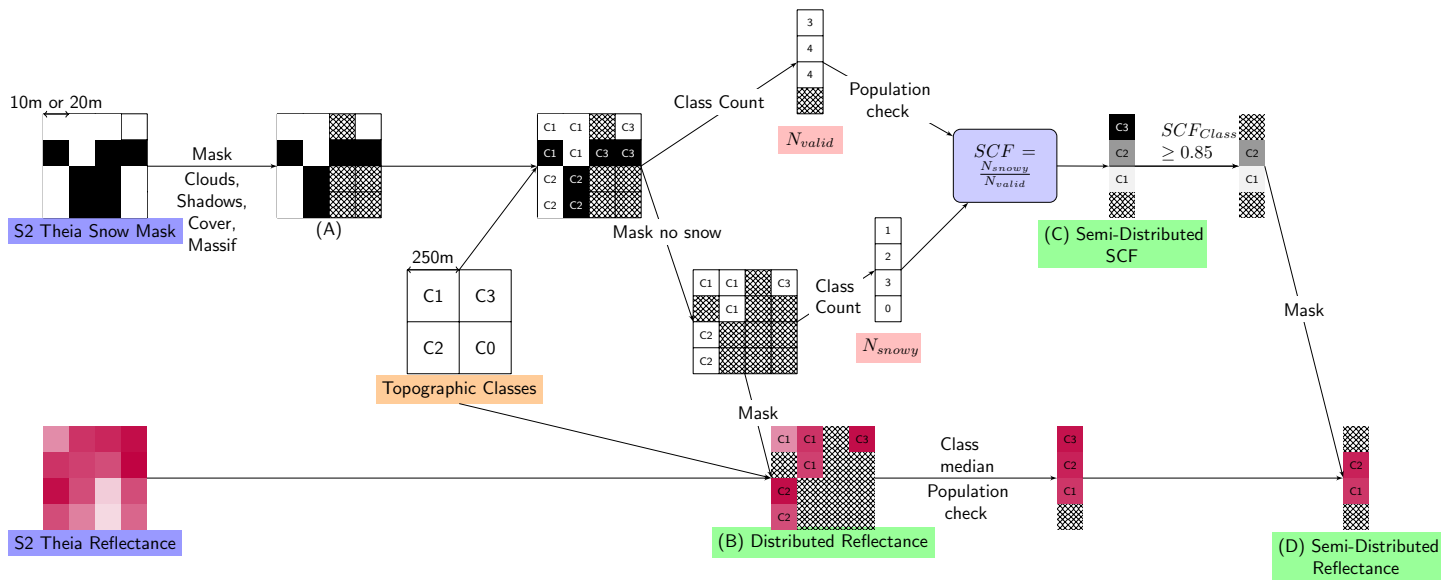


Figure 6: Flowchart of the conversion of Sentinel-2 products (purple) to semi-distributed data (green), using the Topographical Classification (orange) from Sec. 3.1.1.

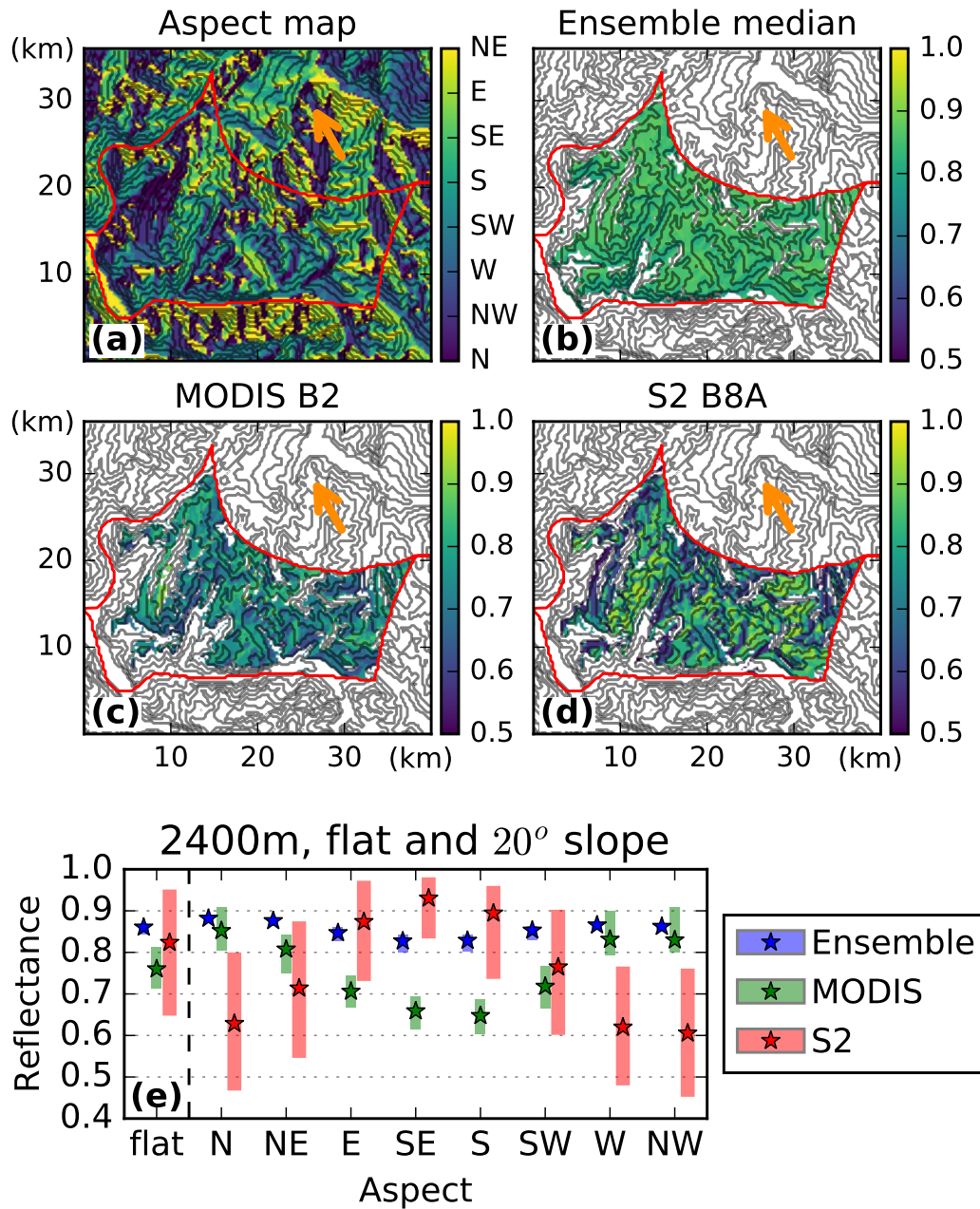


Figure 7: Map of aspect in the Grandes-Rousses (a), and comparison of the 3 reflectance products in the NIR (860nm) on 2017-02-18, 10:00 am: ensemble median (b), semi-distributed MODIS band 2 (c) and S2 Band 8A (2017-02-19, 11:00am) (d). Boxplots (quartiles and medians) for the ensemble (blue), distributed MODIS (green) and S2 (red) in the 2400m, flat and 20° slope classes. On the maps (a-d), the contours denote the model's 300m elevation bands, orange arrows show the approximate sun direction and shadows are masked.

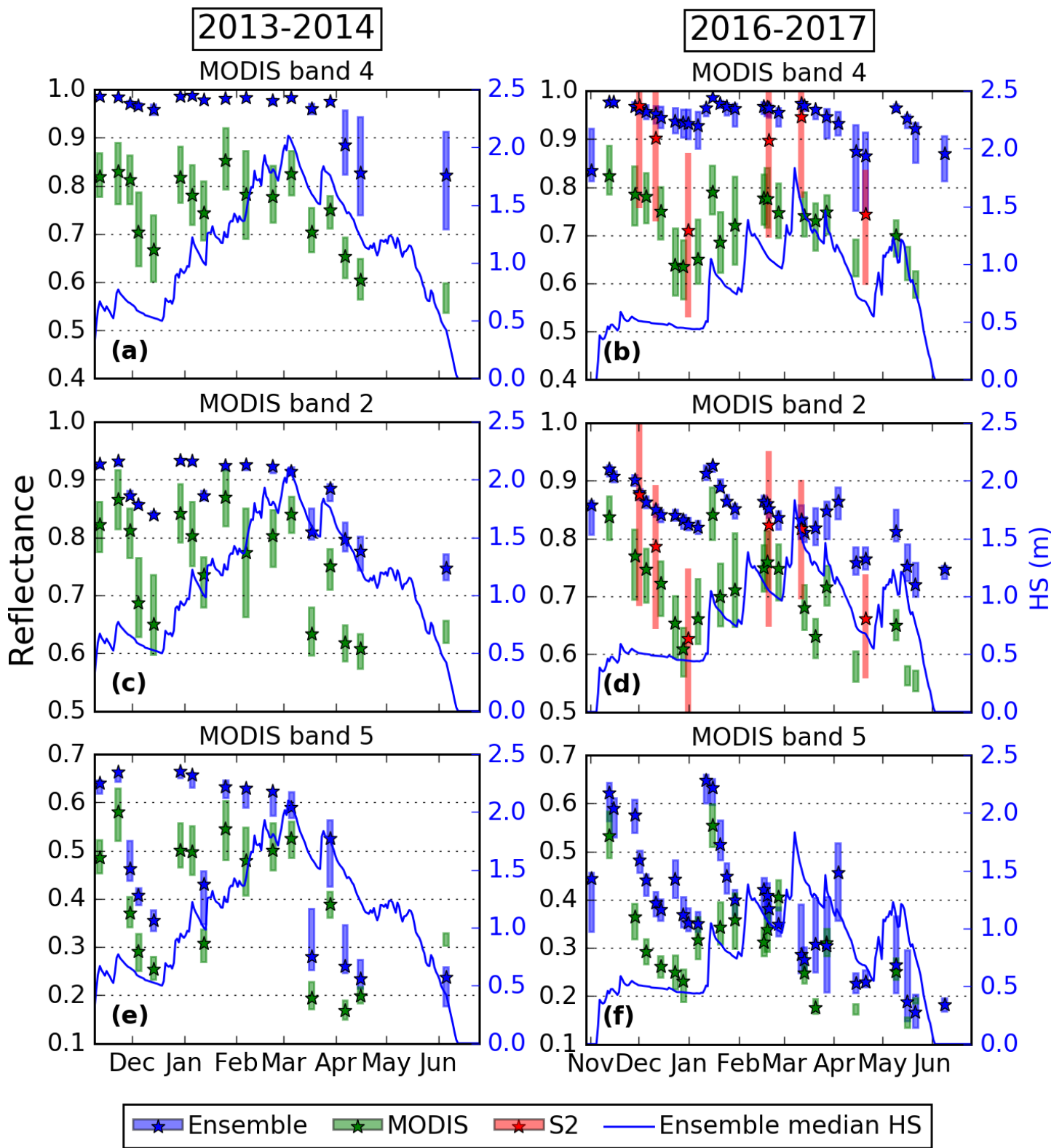


Figure 8: 2013-2014 (a,c,e) and 2016-2017 (b,d,f) timeseries of reflectance in MODIS band 4 (a,b), 2 (c,d) and 5 (e,f) for the three different products (ensemble in blue, MODIS in green, S2 in red). The stars denote the median of the ensemble and the semi-distributed satellite products. The boxes shows the ensemble and distributed satellite products quartiles. See Tab.1 for the wavelengths and S2 corresponding bands. The blue line denotes the ensemble median Height of Snow (HS).

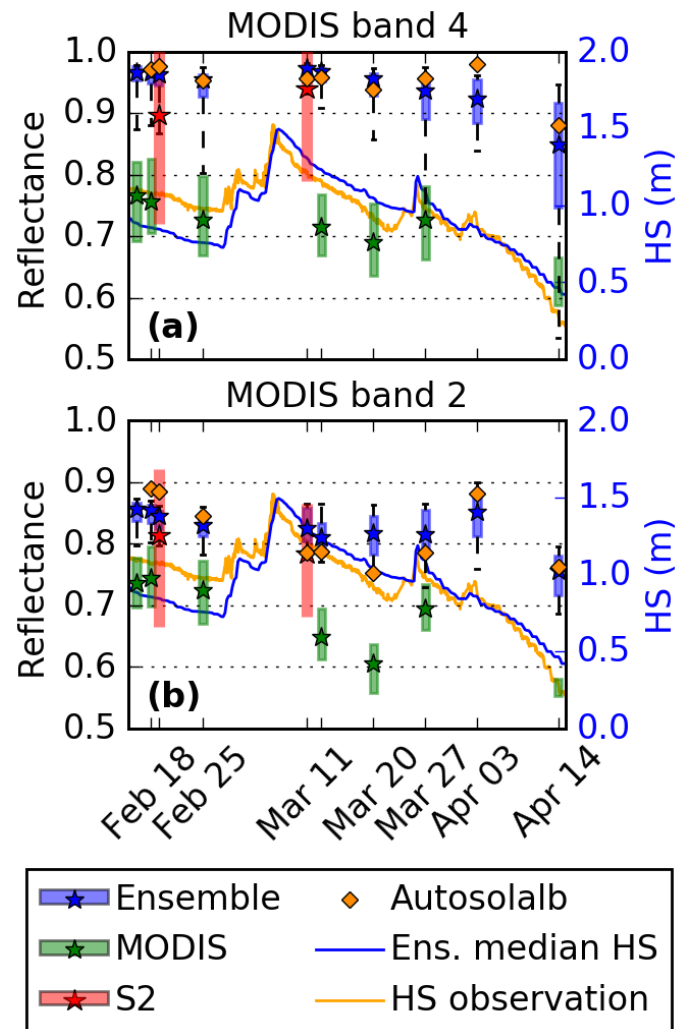


Figure 9: Same as Fig. 8, in 2100 m.a.s.l flat class for 2016-2017 winter in MODIS band 4 (a) and 2 (b). In addition, Lautaret data from Autosolalb (orange diamonds), and observed HS (orange line) are displayed. Note that bars denote the ensemble 5-95th percentiles.

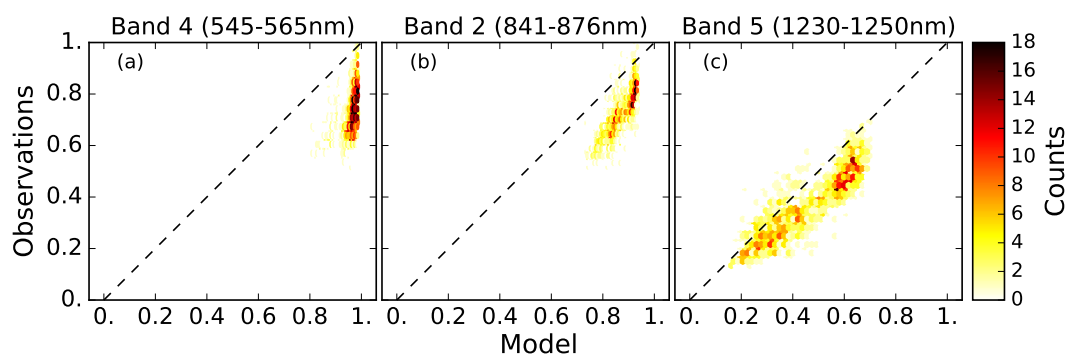


Figure 10: Semi-distributed MODIS observations in band 4 (a), 2 (b) and 5 (c) against ensemble median (density in color), for the 45 topographical classes within 1800-3000m and 0-20 slope, for all the observation dates of 2013-2014 and 2016-2017 snow seasons.

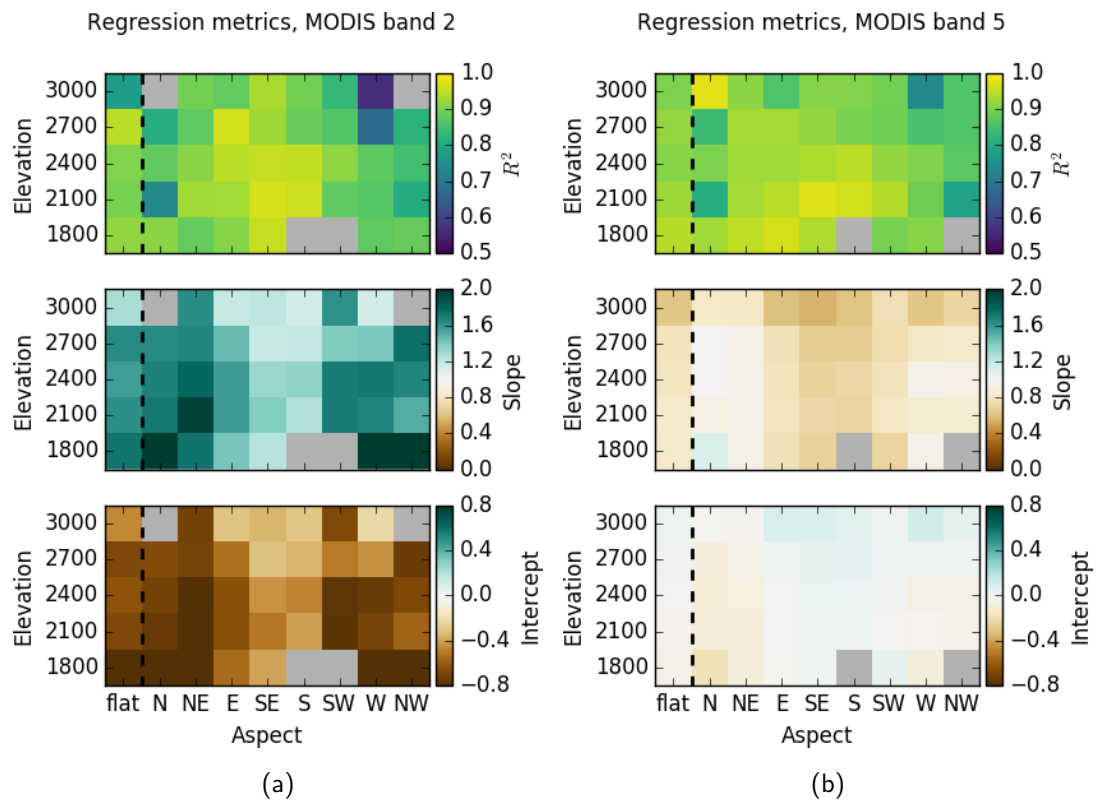


Figure 11: Linear regression statistics (upper panel : squared Pearson correlations R^2 , center panel : regression slope, bottom panel : regression intercept) in band 2 (a) and 5 (b) between the time series of ensemble median and semi-distributed observations for the 45 classes within 1800-3000 m.a.s.l and 0-20 degrees of slope, during 2013-2014 and 2016-2017 snow seasons. Regressions with p-values > 0.01 and less than 6 dates overall are greyed out.

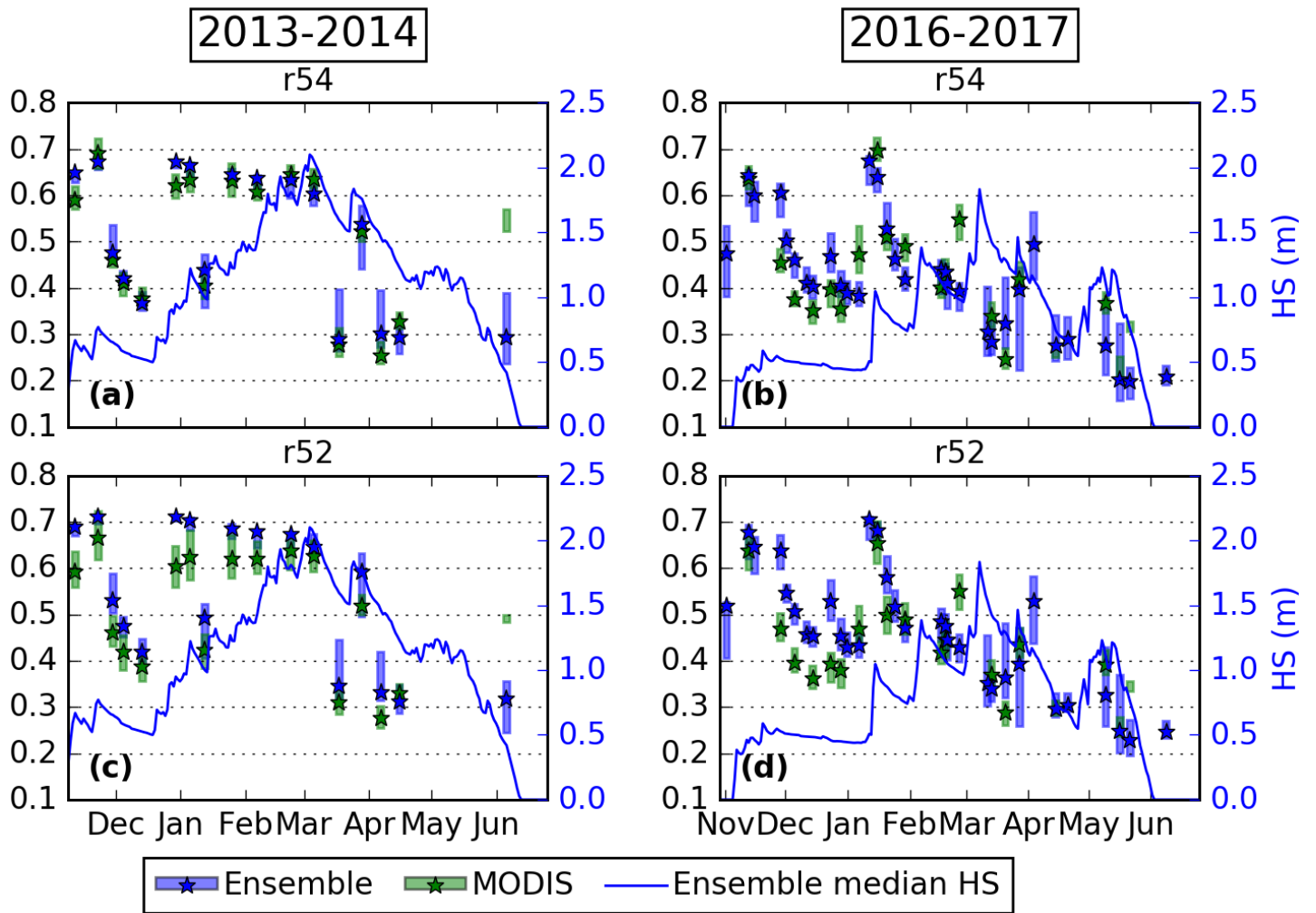


Figure 12: Same as Fig. 8 for band ratios $r54$ (a,b) and $r52$ (c,d).

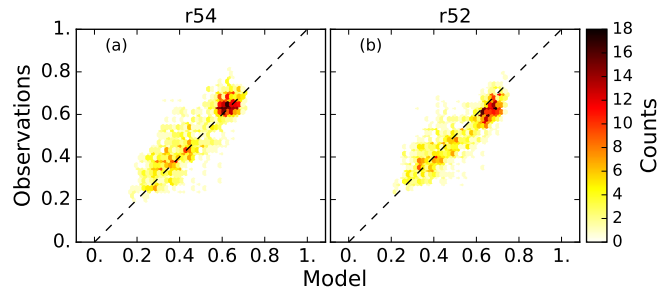


Figure 13: Same as Fig. 10 for r54 (a) and r52 (b).

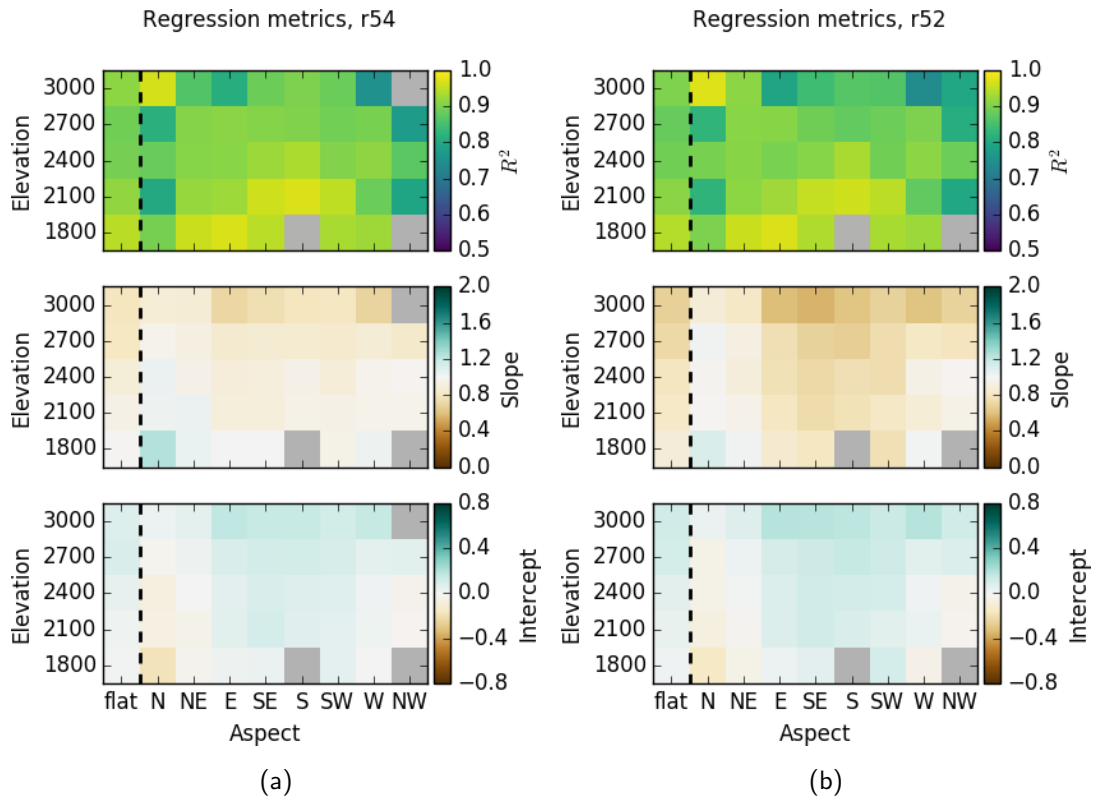


Figure 14: Same as Fig. 11a for r54 (14a) and r52 (14b).

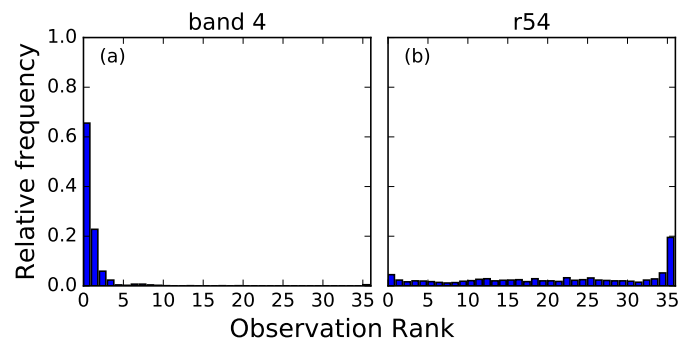


Figure 15: Rank diagrams for the semi-distributed MODIS observations in band 4 (a) and r54 (b) within the ensemble for all classes between 1800 and 3000 m.a.s.l. and between 0 and 20° of slope, and all dates of 2013-2014 and 2016-2017 snow seasons (1009 occurrences).

Appendix A. Table of observation dates

Date	MODIS	S2	Autosolalb	Date	MODIS	S2	Autosolalb
2013-11-11 11:00	X			2016-12-14 10:00	X		
2013-11-22 10:00	X			2016-12-23 10:00	X		
2013-11-29 10:00	X			2016-12-28 11:00	X		
2013-12-04 11:00	X			2016-12-31 10:00		X	
2013-12-13 11:00	X			2017-01-06 11:00	X		
2013-12-29 11:00	X			2017-01-11 11:00	X		
2014-01-05 11:00	X			2017-01-15 11:00	X		
2014-01-12 11:00	X			2017-01-20 11:00	X		
2014-01-25 10:00	X			2017-01-24 10:00	X		
2014-02-06 11:00	X			2017-01-29 11:00	X		
2014-02-22 11:00	X			2017-02-16 11:00	X		X
2014-03-05 10:00	X			2017-02-18 10:00	X		X
2014-03-17 11:00	X			2017-02-19 11:00		X	X
2014-03-28 10:00	X			2017-02-25 10:00	X		X
2014-04-06 10:00	X			2017-03-11 11:00		X	X
2014-04-15 10:00	X			2017-03-13 10:00	X		X
2014-06-05 11:00	X			2017-03-20 11:00	X		X
Winter 2016-2017				2017-03-27 11:00	X		X
2016-11-01 11:00		X		2017-04-03 11:00		X	X
2016-11-12 10:00	X			2017-04-14 10:00	X		X
2016-11-15 11:00	X			2017-04-20 10:00	X		X
2016-11-28 10:00	X			2017-05-09 10:00	X		
2016-12-01 11:00		X		2017-05-16 10:00	X		
2016-12-05 11:00	X			2017-05-21 11:00	X		
2016-12-11 11:00		X		2017-06-08 11:00	X		

Table A.1: Summary of observation dates for MODIS, S2 and Autosolalb sensors over 2013-14 and 2016-2017 winters. Time is given for the corresponding closest model output time step (hour).

Appendix B. Intraclass distribution of observations

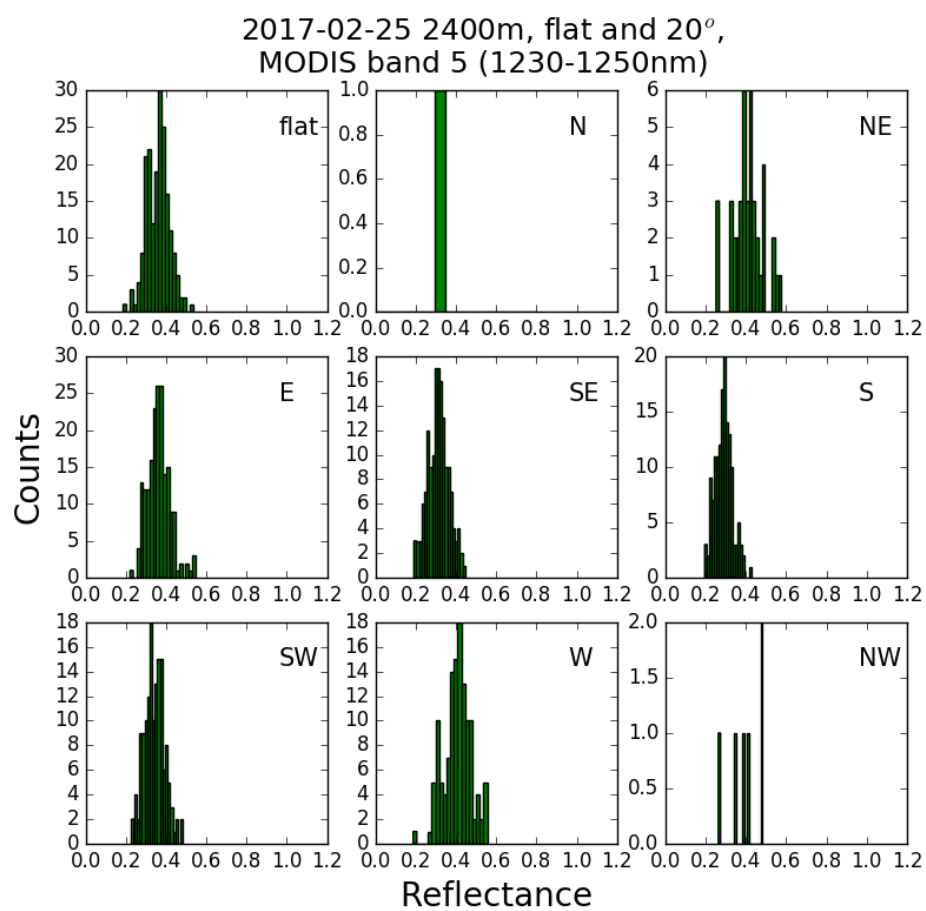


Figure Appendix B.1: Histograms of MODIS band 5 reflectance in flat and 20° slope classes at 2400m on 2017, February the 25th, 10:40am.